Characterization and Modeling of Size Effect on the Performances of 0.10 μm RF MOSFETs for SOC Applications

Yo-Sheng Lin[+], Hsin-Yuan Tu, Hong-Wei Chiu, and Shey-Shi Lu, *Senior Member, IEEE*

[+]Department of Electrical Engineering, National Chi-Nan University, Puli, Taiwan, R.O.C.
Tel: 886-4-92910960 ext.4101, Fax: 886-4-92917810, Email : stephenlin@ncnu.edu.tw
Department of Electrical Engineering, National Taiwan University, Taipei, Taiwan, R.O.C.

Abstract — In this paper, we demonstrate the size effect on the DC and RF performances of 0.10 μm RF MOSFETs for SOC applications. Our results show that for RF MOSFETs, the input impedance can be represented by a series RC circuit at low frequencies and a "shifted" parallel RC circuit at high frequencies. In addition, the output impedance can be represented by a "shifted" series RC circuit at low frequencies and a "shifted" parallel RC circuit at high frequencies. The appearance of the kink phenomenon of scattering parameters S_{11} and S_{22} in a Smith chart is caused by this inherent ambivalent characteristic of the input and output impedances. It was found that an increase of device's width (or g_m) enhances the kink effect of S_{11} and S_{22}. The present study enables RF engineers to understand the behaviors of S-parameters more deeply, and hence are helpful for them to create a fully scalable CMOS model for SOC applications.

I. Introduction

The kink phenomenon in scattering parameter S_{22} of RF MOSFETs/MESFETs and BJTs/HBTs, which has been explained quantitatively [1]-[2], can be seen frequently in the literature [3]-[4]. However, the kink phenomenon in scattering parameter S_{11} of RF MOSFETs or BJTs has never been reported. In this paper, the kink phenomenon in S_{11} of RF MOSFETs is reported and explained quantitatively for the first time. It was found that an increase of device's width enhances the kink effect. The kink phenomenon of S_{11} of RF MOSFETs is explained by deriving the input impedance (or admittance) of a four-terminal MOSFET under the measurement conditions of S-parameters.

From the point of view of device physics, the appearance of the kink phenomenon of S_{11} and S_{22} has nothing to do with any non-ideal characteristics due to device defects or trapping of carriers. Actually, it results from the interaction of C_{gs}, C_{gd}, C_{ds}, g_m, C_{bs}, C_{bd}, g_{mb}, and R_b. etc. If any of the previous terms results in a decrease of r and increase of g, then the kink phenomenon will become more prominent. In this paper, devices fabricated by a 0.10 μm RF CMOS technology was used to study the size effect (or g_m) on the kink phenomenon of S_{11}.

II. DC Characteristics of 0.10 μm RF MOSFETs

Key layout parameters, and DC and RF performances at V_{DS}=V_{GS}=1.2V of nMOS devices A-E studied in this work are summarized in Table I. Note that the corresponding pMOS devices A'-E' with the same sizes as the nMOS devices listed in Table I were also fabricated, but are not listed here. Devices A-D are typical 0.10 μm RF nMOSFETs for low-power RF-IC applications, while device-E is typical 0.10 μm low-leakage nMOSFET for low-power and high-speed SRAMs applications. The only difference in process between devices A-D and device-E is the dosage of channel implantation. As shown in Table I, the normalized DC characteristics of devices A-D are nearly the same, so only DC characteristics of device-D will be discussed in the following.

The measured DC characteristics of device-D are shown in Fig. 1(a)-(d). Fig. 1(a) shows typical I_{DS}-V_{DS} characteristics. Fig. 1(b) shows typical I_{off}-V_G characteristics under various reverse body biases (V_B). Fig. 1(c) shows the measured I_{off}-V_B characteristics under various temperatures. For 250/150 pA/μm nominal off-state currents (I_{off_nom}) @1.1V_{CC}=1.32 V, n/pMOS with excellent 580/235 μA/μm nominal drive currents @V_{CC} =1.2V were achieved. In addition, if additional channel implantations are done, 15/10 pA/μm I_{off_nom} @1.1V_{CC}=1.32V for n/pMOS can be achieved. The corresponding driving currents @V_{CC} =1.2V were 430/175 μA/μm for n/pMOS, as summarized in Table I. Fig. 1(d) shows the I_{off} components versus temperature characteristics. As can be seen, the I_{EDT} leakage current was kept to be under the 10% of I_{off_max} of device-E (50 pA/μm) at room temperature in order to meet the stringent I_{off_nom} requirement of 15 pA/μm. This ensures the possibility of tuning device-D to device-E without the need to increase the oxide thickness.

III. RF Performance of 0.10 μm RF MOSFETs

The measured S_{11} and S_{22} characteristics of device A-D are shown in Fig. 2(a)-(d). Fig. 2(a) and 2(b) show the measured S_{11} and S_{22} characteristics in a Smith chart,

0-7803-7694-3/03/$17.00 © 2003 IEEE

respectively. Fig. 2(c) and 2(d) show the measured $|S_{11}|$ and $|S_{22}|$ characteristics in a Bode plot, respectively. Based on Fig. 2 and the summarized results of S_{11} and S_{22} in table I, we can conclude that the kink phenomenon in S_{11} of RF MOSFETs can be interpreted in terms of poles and zeros only when the device's gate-width is not too small. In addition, the kink phenomenon in S_{22} of RF MOSFETs can be interpreted in terms of poles and zeros only when the device's gate-width is within a middle range. As shown in Table I, the kink phenomenon in S_{22} of device-D cannot be interpreted in terms of poles and zeros because its corresponding R_{ds} is too small (close to 50Ω) due to large gate-width (see Fig. 2(b)), so there is no local minimum in the Bode plot of S_{22} (see Fig. 2(d)).

On the other hand, we can see that an increase of device's width enhances the kink effect of S_{11} and S_{22}. In addition, the kink-frequency first increases then decreases with the increase of gate width. These trends can be explained by the following derived input-impedances both at low frequencies and at high frequencies. At low frequencies, the input impedance can be simplified to a simple series RC circuit as follows:

$$Z_{in} \approx R_g + R'_{gs} \cdot \left(\frac{C'_{gs}}{C'_{gs}+C_M}\right)^2 + R_M \cdot \left(\frac{C_M}{C'_{gs}+C_M}\right)^2 + \frac{1}{j\omega(C'_{gs}+C_M)}$$
$$\approx r_s + \frac{1}{j\omega C_s} \quad (1)$$

where $R_M = [R_L(C'_{ds}+C'_{gd}) + R'_{gd}C'_{gd}]/C_M$, $C_M = C'_{gd}(1 + g'_m R_L)$, in which $R_L = R'_{ds} \| (R_d + Z_O)$. In addition, at high frequencies, the input impedance can be simplified to a "shifted" parallel RC circuit as follows:

$$Z_{in} \approx R_g + \left\{\frac{C'_{gd}+C'_{gd}g'_m R_L}{R_L(C'_{gd}+C'_{ds}+C'_{db}) + R'_{sub}C'_{db} + R'_{dg}C'_{gd}} + j\omega(C'_{gs}+C_p)\right\}^{-1}$$
$$\approx R_g + (g_p + j\omega C'_p)^{-1} \quad (2)$$

where $C_p = [R_L C'_{gd}(C'_{db}+C'_{ds}) + C'_{db}R'_{sub}C'_{gd}(1+g'_m R_L)]/[R_L(C'_{gd} + C'_{db}+C'_{ds}) + (C'_{db}R'_{sub}+C'_{gd}R'_{gd})]$.

Fig. 3(a) shows the adopted small-signal equivalent circuit model. Fig. 3 (b) shows the measured and modeled S-parameters of device-C. The extraction of parameters was based on the method introduced in Ref. [5]. Fig. 3(c) shows the current gain and MSG/MAG versus frequency characteristics of device-C. Very good f_T and f_{max} of 43 GHz and 33 GHz, respectively, were attained.

Fig. 4(a) shows P_{in} versus P_{out}, G_p and PAE characteristics of devices B-D. Fig. 4(b) shows P_{out} versus PAE and G_p characteristics of devices B-D. Fig. 4(c) shows V_{GB} versus P_{out} characteristics under P_{in}=5 dBm of devices B-D. Fig. 4(d) shows the two-tone third-order intermodulation interception point OIP3 of device-D at 2.4 GHz and 5.2 GHz. As can be seen from Fig. 4(a)-(d), very good power performance has been achieved. In addition, no any anomaly was found. These results show the 0.11 μm CMOS technology is very suitable for power applications.

IV. Conclusions

The size effect on the performance of 0.10 μm RF MOSFETs, especially on the anomalous kinks observed in S_{11} and S_{22} have been analyzed. In conclusion, the "anomalous kink" is a "normal behave" of S_{11} and S_{22}. From the point of view of device physics, the appearance of the kink has nothing to do with any non-ideal characteristics due to device defects or trapping of carriers. Actually, it results from the interaction of C_{gs}, C_{gd}, C_{ds}, g_m, C_{bs}, C_{bd}, g_{mb}, and R_b, etc. If any of the previous terms results in a decrease of r and increase of g, then the kink phenomenon of S_{11} and S_{22} will become more prominent.

References

[1] S. S. Lu, C. C. Meng, T. W. Chen and H. C. Chen, *IEEE Trans. on Microwave Theory and Techniques*, vol. 49, no. 2, pp. 406-409, Feb. 2001.

[2] H. Y. Tu, Y. S. Lin, P. Y. Chen, and S. S. Lu, *IEEE Trans. on Electron Devices*, vol. 49, no. 10, pp.1831-1833, Oct. 2002.

[3] Y. Aoki, and Y. Hirano, "High-Power GaAs FETs," *High Power GaAs FET Amplifiers*, p. 81, 1993

[4] T. Takahashi, S. Sasa, A. Kawano, T. Iwai, and T. Fuji, *IEEE, IEDM, Tech. Dig.*, 1994, pp. 191-194.

[5] F. X. Pengg, *2002 Radio Frequency Integrated Circuits Symposium*, pp. 355-358.

Table I. Key layout parameters, and DC and RF performances at V_{DS}=V_{GS}=1.2V of devices A-E studied in this work.

	Device-A	Device-B	Device-C	Device-D	Device-E
width (μm)	6	36	72	144	144
number of finger	1	6	18	18	18
gate length (μm)	0.1	0.1	0.1	0.1	0.1
I_{ds_nom} (μA/μm)	575	577	579	580	430
V_{t_nom} (V)	0.3	0.3	0.3	0.3	0.44
I_{off_nom} (pA/μm)	290	292	295	296	15
I_{off_max} (pA/μm)	1000	1000	1000	1000	50
kink freq. of S_{11} (GHz)	12.2	24.6	21.8	19.4	NA
local minimum of $\|S_{11}\|$ (GHz)	28.2	24.6	21.8	19.4	NA
kink freq. of S_{22} (GHz)	12.8	17	13.8	10	NA
local minimum of $\|S_{22}\|$ (GHz)	28.2	17	13.8	NA	NA
f_T (GHz)	< 0.2	29	43	43	NA
f_{max} (GHz)	5	31	33	33	NA

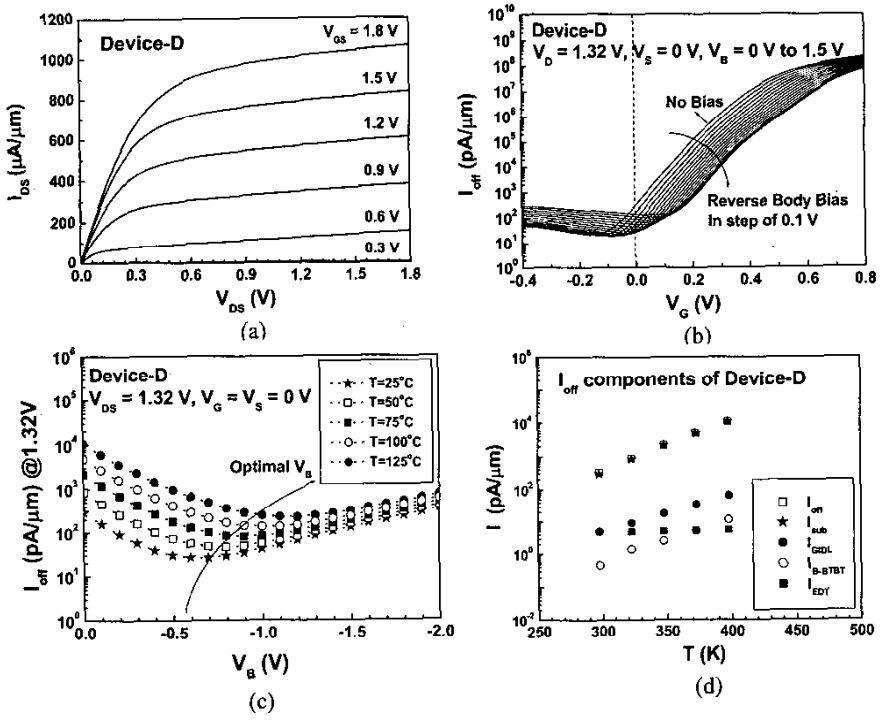

Fig. 1 The measured DC characteristics of device-D. (a) I_{DS} versus V_{DS} characteristics, (b) I_{off} versus V_G characteristics, (c) I_{off} versus reverse body bias characteristics under various temperatures, and (d) I_{off} components versus temperature characteristics.

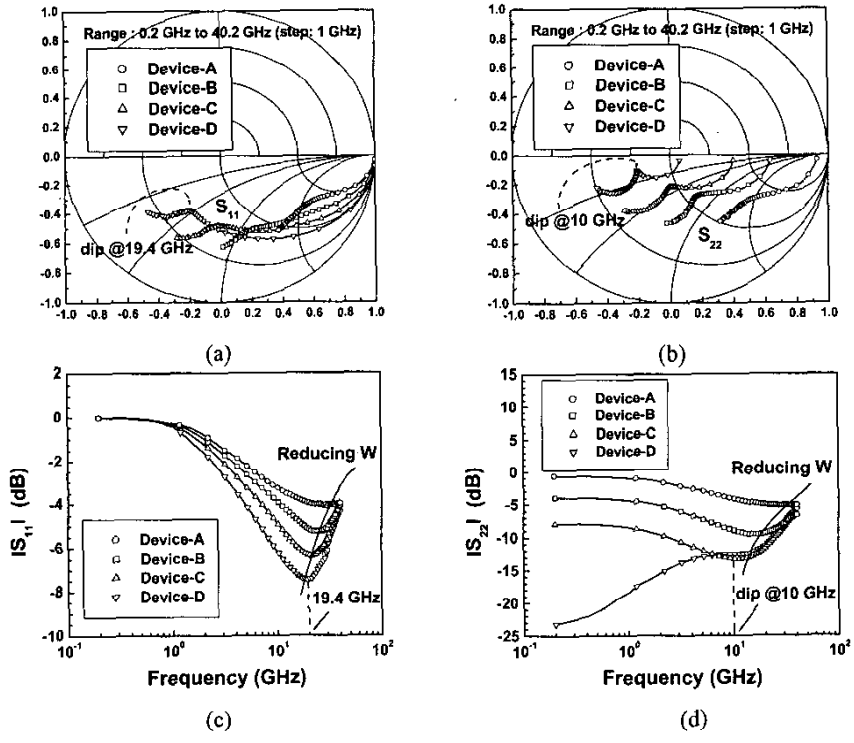

Fig. 2 (a) The measured S_{11} of devices A-D, (b) the measured S_{22} of devices A-D, (c) $|S_{11}|$ versus frequency characteristics of devices A-D, and (d) $|S_{22}|$ versus frequency characteristics of devices A-D.

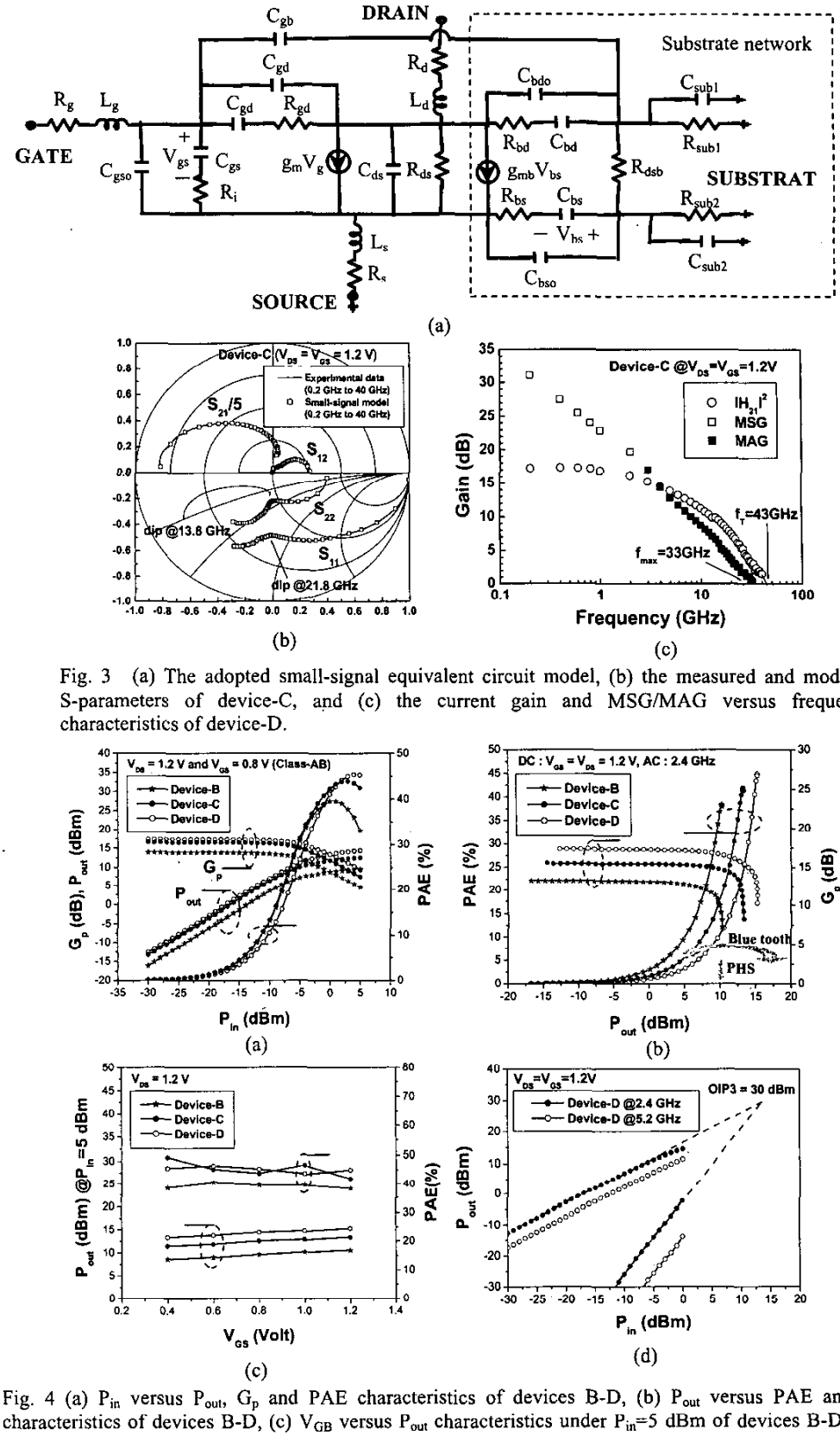

Fig. 3 (a) The adopted small-signal equivalent circuit model, (b) the measured and modeled S-parameters of device-C, and (c) the current gain and MSG/MAG versus frequency characteristics of device-D.

Fig. 4 (a) P_{in} versus P_{out}, G_p and PAE characteristics of devices B-D, (b) P_{out} versus PAE and G_p characteristics of devices B-D, (c) V_{GB} versus P_{out} characteristics under P_{in}=5 dBm of devices B-D, and (d) two-tone third-order intermodulation interception point OIP3 of device-D at 2.4 GHz and 5.2 GHz.